EI SEVIER

Contents lists available at ScienceDirect

Chemical Geology

journal homepage: www.elsevier.com/locate/chemgeo



Using a mathematical model of a weathering clast to explore the effects of curvature on weathering



M.I. Lebedeva ^{a,*}, P.B. Sak ^b, L. Ma ^c, S.L. Brantley ^a

- ^a Earth and Environmental Systems Institute and Department of Geosciences, The Pennsylvania State University, University Park, PA 16802, USA
- ^b Department of Earth Sciences, Dickinson College, Carlisle, PA 17013, USA
- ^c Department of Geological Sciences, University of Texas at El Paso, El Paso, TX 79968, USA

ARTICLE INFO

Article history: Received 14 February 2014 Received in revised form 9 March 2015 Accepted 19 March 2015 Available online 9 April 2015

Editor: Michael E. Böttcher

Keywords:
Weathering rind
Reactive transport modeling
Curvature and weathering
Stefan problem

ABSTRACT

For the first time, we show that rind thicknesses developed on surfaces of a clast with different values of curvature can be used to estimate the duration of clast weathering. To obtain an analytical expression for the velocity of the curvilinear weathering front on a clast of arbitrary shape, we approximate our previous multi-mineral reactive-diffusion model and explore a simplified 2-D model numerically and analytically.

Our analysis documents that with increasing curvature of the weathering front, the mathematical description of weathering advance is equivalent to that derived for advection as the dominant solute transport mechanism, even for the case where transport is occurring by diffusion only. Specifically, for a curvilinear weathering front with constant curvature K < 0, diffusivity (D), and porosity (ϕ) , the normal component of the weathering advance rate can be calculated using an advection-like term where the advection velocity v can be expressed as $v = D\phi | K|$. Therefore, at points along the rind–core interface with K < 0, rind thickness is directly proportional to the absolute value of the curvature of the core–rind interface. The reaction front thickness also increases with K. These inferences are in agreement with field observations. This quantitative analysis allows an assessment of the duration of weathering if certain parameters are known. For example, using the difference in curvature observed at two positions for a clast that weathered in Guadeloupe $(0.12 \text{ mm}^{-1} \text{ and } 0.018 \text{ mm}^{-1})$ and the corresponding rind thickness difference (35.8 mm and 20.6 mm), we estimated the duration of weathering to be about 118 ky, which is consistent with the weathering ages previously determined by U-series isotope disequilibrium.

Published by Elsevier B.V.

1. Introduction

Weathering rinds have been described on clasts since at least the 1960s (Cernohouz and Solc, 1966), and the rates of formation of these rinds have been used to assess the duration of weathering (Colman and Pierce, 1981; Colman, 1982; Kirkbride, 2005; Kirkbride and Bell, 2010). For example, Sak et al. (2004) measured weathering rind thicknesses on basaltic clasts from terraces of constrained geologic age to evaluate the rate of weathering rind advance, i.e. the velocity (distance/time) of advance of the interface between core and rind inward into the unaltered core of the clast. In that work, the rind was defined as the layer of clast material that enveloped the unaltered core protolith. They calculated the mean of observed rind thickness on clasts weathered for different exposure times and fitted these data to rate laws of weathering that are parabolic (i.e., the rind thickness $L = const \cdot \sqrt{t}$ where t is the time and const stands for a constant) or linear (rind thickness $L = const \cdot t$). For the low-porosity (basaltic) clasts that were under study, reactive transport is dominated by solute diffusion (Neretnieks, 1980; Steefel and Lichtner, 1994), and such diffusion is not generally thought to be well explained with a linear transport law. Instead, diffusion is better described by a parabolic rate law (Lichtner, 1988). They nonetheless concluded on the basis of observations of weathered clasts that a linear law was adequate to describe the rind evolution. The growth-rate curve could also have been fit by a more complex law that is neither parabolic nor linear.

In general, most 1-D models used for modeling weathering clasts (Navarre-Sitchler et al., 2011) are based on the assumption of an infinite weathering domain whereas the size of an actual clast is finite. Moreover, observations of rind–core interfaces on basaltic–andesitic clasts (Sak et al., 2010; Ma et al., 2012) reveal that they are generally curved (or, in mathematical parlance, "curvilinear"). Importantly, curvature affects the rate of material alteration, i.e., the weathering advance rate (Ortoleva et al., 1987; Sak et al., 2010; Ma et al., 2012; Lebedeva and Brantley, 2013; Reeves and Rothman, 2014). Many researchers have investigated the rate of advance of weathering (Lichtner, 1988; Steefel and Lichtner, 1994; Wang et al., 1995; Soler and Lasaga, 1998; White, 2002; Zaraisky et al., 2002; Oguchi, 2004; Lebedeva et al., 2007; Sidborn and Neretnieks, 2007) but these authors have analyzed weathering advance rates for planar reaction interfaces, i.e., where the regolith–bedrock or rind–core boundary is characterized by a curvature equal to zero. For

^{*} Corresponding author.

example, Oguchi (2004) analyzed a planar weathering interface for clasts and obtained a parabolic law for the time dependence of rind thicknesses.

We present here a quantitative investigation of the complex behavior of a curvilinear weathering front and how it affects the rate of weathering advance of the rind-core boundary over time. We seek to understand the thickness of the rind material (rind thickness), the rate of growth of the rind (weathering advance rate), and the thickness of the core-rind interfacial layer where the concentration of dissolving mineral changes (the weathering or reaction front). Our approach differs from a recent treatment (Reeves and Rothman, 2014) which was set up following our model (Lebedeva et al., 2010). For example, Eqs. (3)–(4)(presented later) were rewritten from our work (Lebedeva et al., 2010) by Reeves and Rothman (2014) in the spherical system of coordinates, i.e., transforming them to 1-D equations. To investigate the problem, Reeves and Rothman (2014) treated a version of the well-known spherical Stephan problem (Hill, 1987) assuming that the latter approximates the diffusion-reaction equations in the original model (Lebedeva et al., 2010). The Stephan problem formulated for spherical symmetry is a 1-D problem which has been treated in several publications from various fields (e.g. Entchev et al., 2001). Reeves and Rothman (2014) used an approximate solution of the symmetrical spherical problem (Hill, 1987) to calculate the time evolution of the thickness of the weathering rind on a spherical clast. Reeves and Rothman (2014) do not explore controls on weathering front thickness nor rind thickness as a function of curvature. In fact, their approach cannot treat an arbitrary, non-spherical, rind-core boundary — in other words, a real clast. Here, we present a full chemical treatment of a 2-D model of arbitrary clast based on our previous multi-mineral multicomponent reactive transport model in 1-D (Lebedeva et al., 2007).

This multi-mineral model was used to treat a model rock composition: it included reactions that initiated bedrock alteration (oxidative dissolution of FeO) and formed weathered material (transformation of albite to kaolinite) (see Appendix A). The model bedrock also contained quartz, treated as inert to weathering. In the model, components in the pore fluid included O₂, Na⁺, SiO₂, Al(OH)₃, H⁺, OH⁻, Fe²⁺, Fe³⁺ and Cl⁻. Here, this model is simplified further and applied to a non-regular 2-D domain. We are unaware of other publications where a full model has been treated in 2-D domains.

The present paper builds on our previous work. We previously explored a simplified model which is based on an approximation of a numerical simulation of the complex model (Lebedeva et al., 2007). The simplified model was shown to satisfactorily reproduce the thicknesses of zones of mineral alteration, changes in porosity, and velocities of the reaction fronts. Therefore, we applied this model to preliminary 2-D modeling of weathered clasts (Sak et al., 2010) where mineral alteration occurred according to the hypothetical reaction $M_1 + A \rightleftharpoons M_2$ between minerals M_1 , M_2 , and a reactant aqueous species A. Specifically, the model was based on the assumption that the rind increased in thickness as a result of reaction between M_1 and A. We compared our simulations with measurements of rind and reaction front thicknesses. Our simulations documented that both the thicknesses of the weathering rinds and weathering fronts (i.e. thickness of the transition zone where minerals dissolve between core and rind) increased when curvature of the weathering front increased. The first result about weathering rinds was consistent with observations while the latter (about reaction fronts) was not. Although we proposed a partial explanation, this question remained open. Simulations also revealed that the core-rind boundary of an idealized angular and irregularly shaped clast eventually approached the geometry of an ellipse. This was similar to modeled results from investigations of a different phenomenon bubble contraction (Entov and Etingof, 1991) - and this similarity gave us the idea to analyze the similarity of the mathematical models describing these different systems.

We also used the simplified weathering model to investigate weathering across eroding convex-upward hillslopes (Lebedeva and Brantley, 2013). In the latter work we found that regolith became

thickest on the hillslopes where the curvature approached a maximum. We compared this result with our preliminary simulations of weathering clasts and hypothesized that curvature-driven solute transport caused development of the thickest rind (on a clast) or thickest regolith (on a hillslope) precisely at the point where weathering fronts show the highest curvature. Here, we continue numerical investigations of weathering of clasts. Unlike the paper by Sak et al. (2010) we investigate the reaction of albite alteration. Although we considered this reaction previously (Lebedeva and Brantley, 2013), in the 2013 paper we focused on the effect of curvature for landforms, including the effect of advection and erosion. That system was not amenable to analytical investigation. Here we quantify the dependencies of the rind and front thicknesses on curvature. We pursue a simplified approach here that allows us not only to simulate weathering clasts of arbitrary geometry but also to obtain the analytical expressions for the velocity and thickness of the curvilinear weathering front. Thus we resolve the uncertainties described in the earlier paper with respect to how the front thickness depends on front curvature (Sak et al., 2010). Other than the treatments by Ortoleva et al. (1987), Sak et al. (2010), Ma et al. (2012), Lebedeva and Brantley (2013), and Reeves and Rothman (2014), analysis of the effect of curvature on weathering rate has not to our knowledge been previously presented in the geochemical literature.

Outside of geochemical studies, the effect of curvature has been analyzed for various reaction-diffusion systems. For more than a half of a century, scientists have investigated this effect, and for some systems it has been documented both experimentally and mathematically (Markstein, 1951; Knapp and Aris, 1972; Zykov, 1980; Zeldovich, 1981; Keener, 1986; Foester et al., 1988; Grindrod, 1991; Brazhnik and Tyson, 1999; Entchev et al., 2001). While these papers are devoted to different natural phenomena, the papers summarized differential equations that are similar to those in our model. Therefore, the properties of these solutions are similar. Here we apply some of the methods from these contributions to our simple 2-D model of the weathering clast and present numerical solutions to illustrate our results.

2. Model formulation

We developed the simplified model here from the observation that many of the important geochemical attributes of rock weathering are reproduced by simulating a model rock containing only one reactive and one inert mineral (Lebedeva et al., 2010). Previously (Lebedeva et al., 2010; Lebedeva and Brantley, 2013), we analyzed and simulated a parent rock containing reactive albite + inert quartz as it weathered to quartz + albite + kaolinite. We argued that the albite could be conceptualized as any abundant rock-forming mineral that reacts quickly with pore fluids. In fact, we have observed albite-rich feldspar is often the most abundant and reactive mineral during weathering of many igneous rocks (Brantley and White, 2009).

Thus, the model is based on the assumption that weathering can be described by albite (ab) transforming to kaolinite (kao) (Lebedeva et al., 2010):

In the approximate model, we combine all aqueous species in the albite reaction (1) into one thermodynamic component, $\frac{1}{2}\text{Na}_2\text{O}$ $\frac{1}{2}\text{H}_2\text{O}$ 2SiO₂, denoting it as NaSi₂ (Lebedeva et al., 2007). We define the extent of reaction for albite dissolution as

$$\eta = 1 - Q/Q^0, \tag{2}$$

where Q (mol/m³) and Q^0 are the concentration of albite in the weathering material and in the protolith, respectively. We also assume isovolumetric weathering. Notably, under this condition it can be shown that η equals $-\tau$ where τ is the mass transfer coefficient (Brimhall and Dietrich, 1987; Anderson et al., 2002).

The governing equations for the time (t) evolution and spatial (x,y) distribution of the concentration of NaSi₂ in pore fluid, C(x,y,t) (mol/m³), and the extent of reaction, $\eta(x,y,t)$, are as follows:

$$\frac{\partial (\phi C)}{\partial t} = \frac{\partial}{\partial x} \left(D\phi \frac{\partial C}{\partial x} \right) + \frac{\partial}{\partial y} \left(D\phi \frac{\partial C}{\partial y} \right) + j(C, \eta) \tag{3}$$

$$\frac{\partial \eta}{\partial t} = \frac{j(C, \eta)}{Q^0}.$$
 (4)

Eqs. (3) and (4) are defined in the spatial domain $(x, y) \in \Omega$ (i.e. any point with coordinates (x,y) belongs to this domain) which is bounded by the surface Γ of the clast. For the 2-D model, this "surface" is a closed curve, $\Gamma(x,y)=0$, that lies on the plane (x,y). We consider a simplified "cylindrical" clast (base of the cylinder, Ω). This assumption is equivalent to assuming that no variables depend on the third dimension. The initial and boundary conditions are as follows:

$$C(x,y,0) = C^{e}, (x,y) \in \Omega$$

$$Q(x,y,0) = Q^{0}, (x,y) \in \Omega$$

$$C(x,y,t) = C^{R}, (x,y) \in \Gamma.$$
(5)

Here, D (m²/s) is the diffusion coefficient in the aqueous pore fluid reduced by tortuosity and ϕ is porosity:

$$\phi = 1 - \phi_{ab} - \phi_{in} \tag{6}$$

where $\phi_{ab} = QV_{ab}^0$ and ϕ_{in} are albite and the inert (quartz) volume fractions, respectively, and V_{ab}^0 (m³/mol) is the albite specific volume.

Note that one aspect of clast weathering that has been treated in the literature is evolution of porosity. Previous researchers emphasized changes in porosity during rind development (Oguchi, 2004; Navarre-Sitchler et al., 2011). Our treatment does not follow the approach described in either of those papers but it does allow porosity to change during weathering according to Eq. (6) when albite dissolves and the volume fraction ϕ_{ab} changes. We assume that initially porosity within the clast is sufficiently low that solute transport occurs only by diffusion (the first two terms in the right-hand side of Eq. (3)); i.e. we do not take into account advection. In this regard the model presented here differs from our previous models (Lebedeva et al., 2010; Lebedeva and Brantley, 2013).

The reaction rate, j (mol/m³ s), for albite transforming to kaolinite, is approximated using the rate equation derived in our previous work (Lebedeva et al., 2007):

$$j = k(1-\eta)(C^e - C) \tag{7}$$

$$k = 2k_{ab}S_{ab}\Psi. (8)$$

In Eq. (7), k (s^{-1}) is the effective rate constant, and C^e is the concentration of NaSi₂ in pore fluid in equilibrium with albite + quartz + kaolinite. In Eq. (8), k_{ab} is the dissolution rate constant for albite in mol m⁻² s⁻¹ as derived from published laboratory experiments (Chou and Wollast, 1985; Hellmann, 1994), s_{ab} is the specific surface area of albite (in m² m⁻³) in the parent material calculated using a geometric model (see Appendix A). A correction factor, Ψ (m³ mol⁻¹) relates the rate constant for albite dissolution to the effective rate constant that pertains when other minerals are present (see original kinetic functions in Appendix A). For example, the effective rate constant may take into account the pH buffering that couples albite dissolution to other mineral reactions that occur in natural systems (Lebedeva et al., 2007). It is important to note that the model implicitly includes the grain size of albite: the value of s_{ab} is determined by grain size. When grain size increases, s_{ab} decreases.

Finally, C^R is the solute concentration that describes the fluid that enters the clast at its outer boundary. Generally, this concentration is a

function of x, y, and t. This function could be found by solving a reactive transport model of the entire weathering column that contains the clast (i.e. including the soil within which the clast is embedded). Below we will discuss this more complex problem but first we assume a single clast bathed in a fluid with a concentration that is constant in time and space. In addition, we assume that the concentration C^R is much less than the equilibrium concentration, $C^R \ll C^e$.

3. Numerical results

Figs. 1 and 2 show numerical solutions of the Eqs. (3)–(8) for the rectangular and irregular domains (clasts), respectively. The solutions of the 2-D problem were obtained using COMSOL Multiphysics software (COMSOL, 2008). During the simulation, the rind-core boundary rounds and eventually approaches an ellipse-shaped form. A similar result was obtained analytically in quite a different research field, namely an investigation of contracting bubbles (Entov and Etingof, 1991). This work considered curvilinear fronts described by equations different from Egs. (3)-(4). Nonetheless, it can be shown that in the diffusioncontrolled regime – i.e., where kinetics is fast and $k \to \infty$ – the model described in Eqs. (3)–(4) can be transformed to the model for bubbles (Entoy and Etingof, 1991), yielding a similar result: the clast tends to form an ellipse (ellipsoid in 3-D) regardless of the initial weathering domain geometry. This result is true for boundary conditions which are homogeneous and constant in time. For different boundary conditions, clasts could become quite different in shape than ellipsoidal. But this ellipsoidal approximation is useful for preliminary estimations. Corestones of ellipsoidal shape have been observed previously (Hewawasam et al., 2013).

To illustrate the effect of curvature we idealize a weathering domain (clast) as an ellipse (Fig. 3), i.e., the elliptical outer boundary Γ is described by $(x/a)^2 + (y/b)^2 = 1$, where a and b are semimajor and semiminor axes respectively. For example, this idealization could be describing weathering of an angular clast starting from the moment when the rind–core boundary becomes elliptical. Only albite and quartz are present in this domain initially and the value of C^R at the clast boundary is zero. The absolute value of curvature, |K|, is expressed by the equation

$$|K| = \frac{\left| \frac{d^2 y}{dx^2} \right|}{\left(1 + \left(\frac{dy}{dx} \right)^2 \right)^{3/2}} = \frac{a^4 b}{\left(a^4 + x^2 \left(b^2 - a^2 \right) \right)^{3/2}}.$$
 (9)

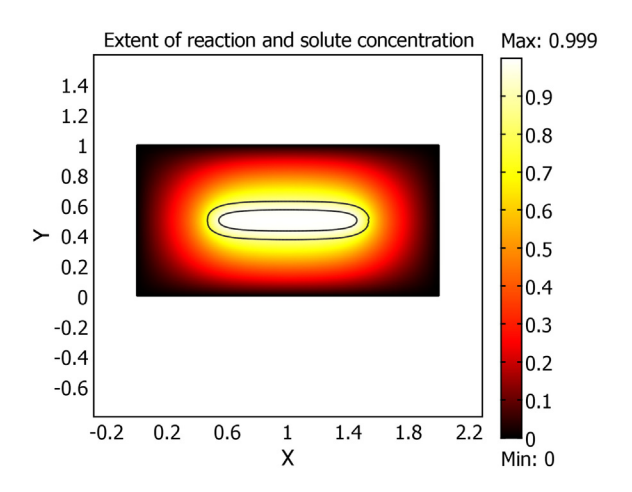


Fig. 1. Simulation of a curvilinear weathering front within a weathering block. The model was completed for $C^R = 0$ everywhere at the outer weathering boundary. Dimensionless time is equal to 0.3. The extent of reaction is plotted as contours for $\eta = 0.9$ (the outer curve where 90% reaction has occurred) and 0.2 (the inner curves where 20% reaction has occurred). The solute concentration is shown by color, where 0 is no solute present and 1 represents chemical equilibration. The simulation documents rounding of corners, as observed in the field for weathering clasts (Sak et al., 2004; Ma et al., 2012). (For interpretation of the references to color in this figure legend, the reader is referred to the web version of this article.)

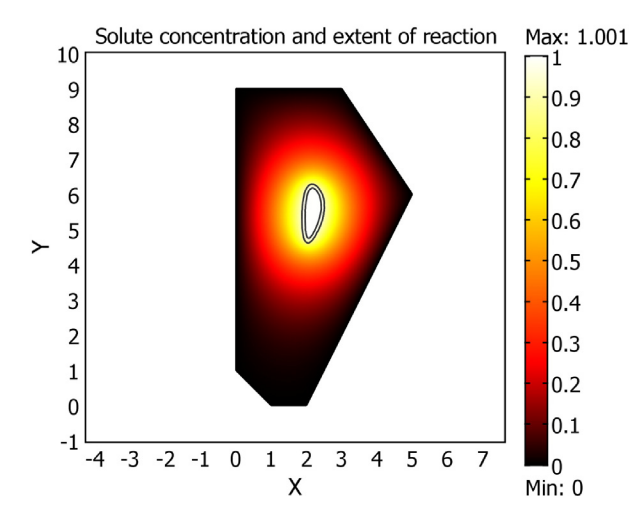


Fig. 2. Simulation of an angular clast. Dimensionless time is equal to 6. Solute concentration in pore fluid is shown with color. Extent of reaction in the rind is presented also as a contour plot with only two contour lines delineated, i.e. $\eta=0.9$ (outer curve) and $\eta=0.2$ (inner curve). The weathering front approaches an elliptical shape with time. These illustrative simulations were performed for arbitrary parameters. Thus, for the chosen length and time scales $L_{sc}=0.034\,$ m and $t_{sc}=L_{sc}^2\alpha^{-1}D^{-1}=7.3\,$ ky, respectively, the dimensional time is equal to 44 ky, maximal horizontal and vertical sizes are equal to 17 cm and 31 cm, respectively. Parameter $\alpha=5\cdot 10^{-5}\,$ is defined in Eq. (26). Other parameters are as follows: $\phi_0=0.1, \phi_{ab}^*=0.4, D=10^{-10}\,$ m² s⁻¹, $k=1.7\cdot 10^{-5}\,$ s⁻¹, $C^R=0$. (For interpretation of the references to color in this figure legend, the reader is referred to the web version of this article.)

At the point (x = 0, y = b), $|K| = b/a^2$ while at the point (x = a, y = 0), $|K| = a/b^2$. For $a \ll b$, the curvature at these points differs appreciably. For this case, therefore, the effect of curvature could be pronounced.

Fig. 3 shows the numerical solution of this problem for a=0.025 m and b=0.075 m after 38 ky. The extent of reaction is plotted as contours for $\eta=0.9$ (i.e., the boundary where 90% reaction has occurred is shown as the outer curve), 0.5, and 0.1 (the inner curves where 50 and 10% reaction have occurred respectively). The solute concentration

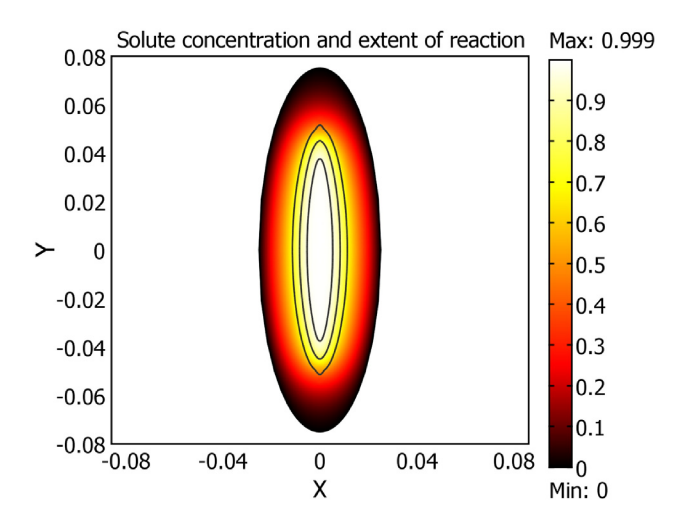


Fig. 3. Contour plots showing the simulated values of the extent of alteration, η , of a weathering rind (three contour curves shown) and solute concentration in pore fluid (color) depicted for one time interval (38 ky). The simulation was conducted for a hypothetical elliptical clast under the condition of solute transport by diffusion only. Contour curves are plotted at $\eta=0.9$, 0.5, and 0.1 (i.e. 90, 50, and 10% reacted). The rind is thicker along the vertical axis of the ellipse where the curvature of the boundary is the largest. The parameters are as follows: a=0.025 m, b=0.075 m, $\phi_0=0.005$, $\phi_{ab}^{*}=0.05$, $D=10^{-10}$ m² s⁻¹, $k=3.8\cdot10^{-7}$ s⁻¹, $C^{R}=0$, $\alpha=5\cdot10^{-5}$. (For interpretation of the references to color in this figure legend, the reader is referred to the web version of this article.)

is shown by color. The absolute value of curvature reaches a minimum, $|K| = 0.0044 \, \mathrm{mm}^{-1}$, at points $(\pm 0.025, 0)$, and reaches a maximum, $|K| = 0.12 \, \mathrm{mm}^{-1}$, at points $(0, \pm 0.075)$. The rind is thicker along the vertical axis of the ellipse where the curvature is at a maximum. Based on the same simulation, Fig. 4(a) documents that the velocity of the weathering front in the direction along the normal to the contour curve is larger where the front curvature is larger. A similar pattern can be observed in the naturally weathered clast described previously (Ma et al., 2012) as shown in Fig. 4(b).

4. Analysis

These simulations demonstrate that curvature of the weathering front affects the weathering front advance velocity. To explain this phenomenon we first summarize how weathering occurs for a planar (K=0) reaction front. These results follow from the analysis of 1-D models that have been published multiple times (Lichtner, 1988; Ortoleva, 1994; Lebedeva et al., 2007):

$$\frac{\partial (\phi C)}{\partial t} = \frac{\partial}{\partial x} \left(D \phi \frac{\partial C}{\partial x} \right) - v \frac{\partial C}{\partial x} + j(C, \eta) \tag{10}$$

$$\frac{\partial \eta}{\partial t} = \frac{j(C, \eta)}{O^0}.\tag{11}$$

These equations describe a planar front, i.e., weathering of a slab where the variables C and η do not depend on the coordinate y.

We have added the advective term to Eq. (10) to compare the evolution of the reaction fronts under diffusion and diffusion-advection. Here v is the Darcy velocity of pore fluid. The theory predicts that the velocity of the weathering front is larger in the presence of advection than when solute transport is by diffusion only (at least for the case when the directions of advection and the advance of weathering coincide). With solute transport by both advection and diffusion, the front moves with approximately constant velocity ω , in direct proportion to v:

$$\omega = v \frac{C^e - C^R}{Q^0}. \tag{12}$$

In contrast, when transport is by diffusion only, the transport slows with time according to the so-called parabolic rate law (Ortoleva et al., 1987; Lichtner, 1988):

$$\omega(t) = \sqrt{\frac{D\phi\left(C^e - C^R\right)}{2Q^0t}}.$$
(13)

For concurrent diffusion and advection, the thickness of a front developed in the presence of advection will generally be larger than that where solute transport is strictly by diffusion.

Fig. 4 documents an important point: curvature of the weathering front results in weathering advance that behaves as if advection were contributing to solute transport, even for the case where transport is occurring by diffusion only. In other words, curvature transforms the time dependence of weathering advance from parabolic to approximately linear.

We can show this effect mathematically using model Eqs. (3)–(4) and a technique described in the literature (Zykov, 1980; Keener, 1986; Grindrod, 1991) (see Appendix B). For a curvilinear weathering front with a constant curvature K, the total normal component of the weathering advance rate, ω_n , is expressed by the following equation:

$$\omega_n = \omega_0 + \omega_K = \omega_0 - \beta K \tag{14}$$

$$\beta = D\phi \left(C^e - C^R \right) / Q^0. \tag{15}$$

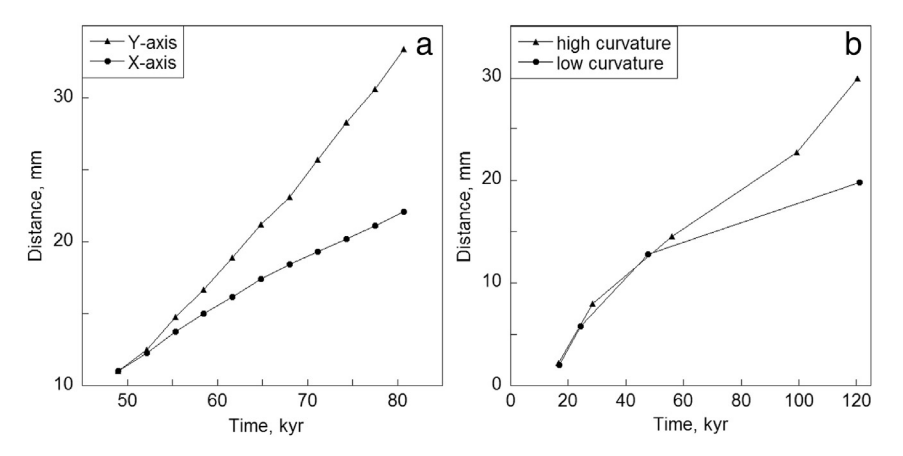


Fig. 4. The time evolution of the thickness of a weathering rind for the elliptical clast (a) calculated along the x-axis (circles) where the absolute value of the initial curvature of the boundary, |K|, equals 0.0044 mm⁻¹, and along the y-axis (triangles) where |K| = 0.12 mm⁻¹. This simulation can be compared to a natural example (b) (Ma et al., 2012) where the time evolution of the weathering rind was obtained along directions normal to the clast boundary at low (circles, |K| = 0.018 mm⁻¹) and high (triangles, |K| = 0.12 mm⁻¹) curvature. We suppose that the elliptical clast was formed during weathering of an angular clast and that at 49 ky the rind thicknesses were equal to 11 mm for both x- and y-axes.

Here ω_0 is the velocity of the plane (rectilinear) front. The additional term, ω_K , is calculated by Eq. (12) with $\nu=-D\phi K$: $\omega_K=-D\phi K(C^e-C^R)/Q^0$.

Thus, the weathering advance rate depends not only on mineralogical composition (Q^0) , solute concentration $(C^e - C^R)$, solute transport characteristics (D, v), and porosity (ϕ) , but also on the curvature of the weathering front K.

Note that the sign of the curvature *K* depends on the choice of the local system of coordinates (see Appendix B). At a given curvature, its effect, i.e. acceleration or deceleration of the reaction front, depends on the direction of front propagation. Therefore, for accurate treatment of any specific case, it is necessary to analyze the effect of curvature taking into account the shape of the reaction front and propagation direction.

It follows from Eq. (14) that for the 2-D curvilinear front, the sign of curvature (the sign of the second derivative in Eq. (9)) is important. The velocity of a front that is convex (K>0) in the direction of the normal to the contour (the curve y(x) where $\eta(x,y)=const$) is less, and the velocity of the concave front (K<0) is greater than the velocity of the plane front (Fig. 5). These results have also been proven experimentally (Foester et al., 1988) but for a different phenomenon, namely, for chemical waves.

Note that Eq. (14) is an approximation, as the curvature of the reaction front generally changes with time. But we can use this equation for time intervals that are short in comparison to the rate that curvature changes. For example, curvature of the weathering front along axis y in Fig. 3 is almost constant in time because initially, $|K| = b/a^2$, but with reaction progress, b varies directly with t due to the "advective effect" of the curvature, and $a \sim \sqrt{t}$ because the advective effect is small. In the literature, analyses of chemical waves have documented more complex nonlinear dependencies for the velocity on curvature (Brazhnik and Tyson, 1999).

Using Eqs. (B.1)–(B.2) from the Appendix B we can derive the dependence of the thickness of the weathering front on curvature in the direction normal to the curvilinear front for the weathering clast case (K < 0). We define the front thickness as the length of the interval where the extent of the reaction, η , changes from zero to unity. We consider the case of K < 0, so the second term in Eq. (B.1) is viewed as the term describing "advective" transport. It has been known (Lichtner, 1988) that for the simplified model Eqs. (10)–(11), the front thickness, h, is approximated by the equation

$$h = 1/q, \ q = \frac{v}{2D\phi} \left(\sqrt{1 + \frac{4D\phi k}{v^2}} - 1 \right).$$
 (16)

Using the expression $v = |K|D\phi$, we obtain for the model (B.1)–(B.2)

$$h = \frac{2}{\sqrt{K^2 + \frac{4k}{D\phi} - |K|}} \approx \frac{D\phi|K|}{k} \tag{17}$$

at $D\phi K^2 \gg 4k$. It follows from Eq. (17) that the front thickness normal to a tangent to the curve at any location is greater in the direction with greater curvature. The same trend was simulated previously (Sak et al., 2010). But the measurements reported for a naturally weathered clast published in that paper did not resolve any systematic variation in the front thickness with curvature. This discrepancy was attributed to the structure of the rind–core boundary.

Nonetheless, we show here that a re-analysis of the results obtained by Sak et al. (2010) documents the trend predicted by Eq. (17). Sak et al. calculated the mass transfer coefficient (Brimhall and Dietrich, 1987) for each element i, τ_i , and inferred from this value the relative fraction of elemental depletion relative to an immobile element in the weathering rind. The mass transfer coefficient of an element such as Ca is related to the extent of reaction of a Ca-containing mineral:

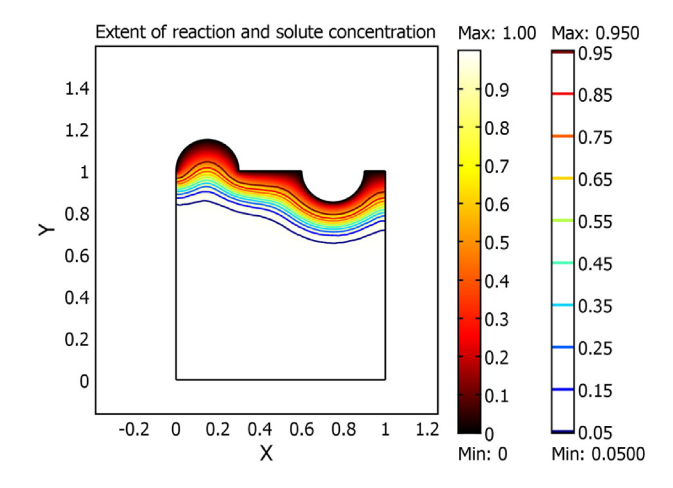


Fig. 5. Model simulations showing the effect of the sign of curvature. Weathering is advancing downward and the reaction front is becoming smoother with time. The curves depict contour lines for the extent of reaction, η . The curvature of the front at the left side is defined here by convention to be negative, K < 0, the curvature in the middle is equal to zero (K = 0), and the curvature at the right is positive, K > 0. The maximal rind thickness is attained at the point of negative curvature on the left.

i.e., $\tau_{Ca} = -\eta$. Fig. 6 shows calculated values of this for different cross-sections of the observed clast. The value of η describes the fraction of an element in the core of the clast that has been lost across the rind due to weathering. As shown in the figure, profiles across the front where it has lower curvature are steeper than the profiles across the highly curved front. Thus, the rind and the reaction front are both thicker at points of high curvature, as long as all the other parameters are the same. For example, the front thickness depends also on porosity and the effective kinetic constant (Eq. (17)). In natural multi-mineral clasts these parameters could differ along with differences in curvature. Such variations may affect the front thickness so that the fronts with greater curvature could be thinner than the fronts with lower curvature in actual clasts.

Eq. (14) can also be applied to real systems. For, example the rind thickness, L, for the elliptical clast should approximately equal

$$L(t) = L_0(t) + |K|\beta t, \ \beta = \frac{D\phi\left(C^e - C^R\right)}{Q^0} \eqno(18)$$

where $L_0(t)$ is the rind thickness for the planar front and |K| is the absolute value of curvature. If L_0 is the same on a natural clast regardless of direction of weathering advance in a given weathering soil, we can derive

$$\beta t = \frac{L_{\text{max}} - L_{\text{min}}}{|K_{\text{max}}| - |K_{\text{min}}|}.$$
(19)

Using Eq. (19) we can estimate either the parameter β — which is important for description of the diffusion front (see Eq. (13)) — or the time t. Differences in $L_{\rm max}$ and $L_{\rm min}$ can therefore be used to estimate the conditions of weathering. For example, for the natural clast analyzed previously (Sak et al., 2010), $L_{\rm max} \approx 35.8\,$ mm, $L_{\rm min} \approx 20.6\,$ mm while $|K_{\rm max}| \approx 0.12\,$ mm $^{-1}$, $|K_{\rm min}| \approx 0.018\,$ mm $^{-1}$. We obtain from Eq. (19) that $\beta t \approx 1.49 \cdot 10^{-4}\,$ m². We can then estimate the parameter β using an average value for $D \sim 10^{-10}\,$ m²/s, $\phi \sim 0.01$, and the ratio ($C^e - C^R/Q^0 \sim 4 \cdot 10^{-5}\,$ as $4 \cdot 10^{-17}$ m²/s (Eq. (18)). Here, we have used data reported previously (Lebedeva et al., 2007) to calculate C^e and assumed $C^R = 0$. Then the duration of weathering is about 118 ky which is in accordance with the result obtained by Ma et al. (2012) using U-series isotope disequilibrium dating.

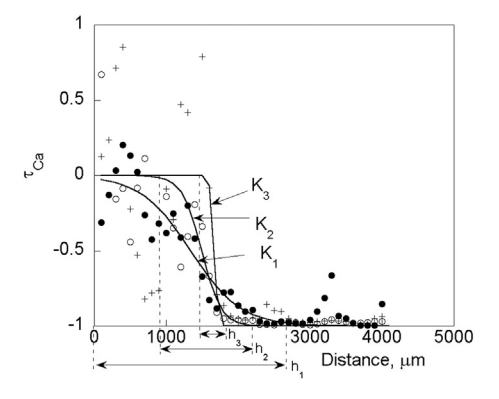


Fig. 6. Elemental mass transfer coefficient τ_{Ca} calculated from analyses of a basaltic clast weathered in Guadeloupe (Sak et al., 2010) plotted as a function of distance from the core–rind boundary. Different symbols refer to different positions along the clast core–rind interface that have different curvature values, K_1 , K_2 , and K_3 ($|K_1| > |K_2| > |K_3|$). The solid curves are curve fits of these data labeled by the curvature of the core–rind boundary. The boundaries of Ca reaction fronts are shown as dashed lines for the three points along the core–rind boundary. Filled circles, open circles, and crosses depict the points with curvature $K_1 = 0.2 \, \text{mm}^{-1}$, $K_2 = 0.05 \, \text{mm}^{-1}$, and $K_3 = 0.03 \, \text{mm}^{-1}$, respectively. Noisiness in the measurements generally relate to the presence of mineral grains in the protolith that vary in Ca content. The distances h_i , i = 1, 2, 3, are the approximate thicknesses of the reaction fronts, i.e. the distances between the intact core where $\tau_{Ca} = 0$ and the completely altered rock where $\tau_{Ca} = -1$.

5. Formation of the curvilinear front and the effect of boundary conditions

A typical weathering and eroding profile on bedrock will consist of fresh unweathered rock overlain by regolith. Infiltration of water into the bedrock is facilitated by joints and other fractures. When considered over long geologic times from the perspective of a constant land surface position, the regolith-to-bedrock profile is characterized by joints and fractures that define the size of rock fragments or corestones that leave the bedrock and move up and out of the system. (In other words, from the perspective of a land surface experiencing erosive loss of material, the regolith stays constant in thickness if weathering advance rate = erosion rate and in that case, rock fragments can be imagined as moving upward through the regolith equivalent to the rate of weathering advance.) With increasing duration of time, these joint-bounded bedrock blocks gradually diminish in size as they remain in the weathering zone, moving upward toward the topsoil (Ruxton and Berry, 1957; Fletcher and Brantley, 2010).

Weathering of each block occurs under a different set of boundary conditions that define the solution chemistry at the block surface. In many cases this leads to formation of curvilinear weathering fronts that differ from the plane fronts modeled using Eqs. (10)–(11). For example, weathering described by a 2-D model of a single rectangular block under boundary conditions (Eq. (5)) has already been shown in Fig. 1. For this simulation, the boundary concentration C^R — the concentration of NaSi₂ in pore fluid at the dissolution boundary — was set to be constant in time and space. The weathering rind within the block eventually approaches the shape of an ellipse.

The boundary conditions at the surface of the clast or block affect the shape and the rate of advance of the weathering front. For example, the block in Fig. 7 was modeled as if it was embedded in an inert porous material: this simulation therefore is meant to help understand how corestones or rock fragments evolve when embedded within a weathering profile. For this simulation, solute concentration at the top of the block was maintained less than the equilibrium concentration $(C^R \ll C^e)$ while the solute concentration at the bottom was maintained close to equilibrium. At the lateral boundaries, solute concentration depends linearly on depth, increasing from the top to the bottom of

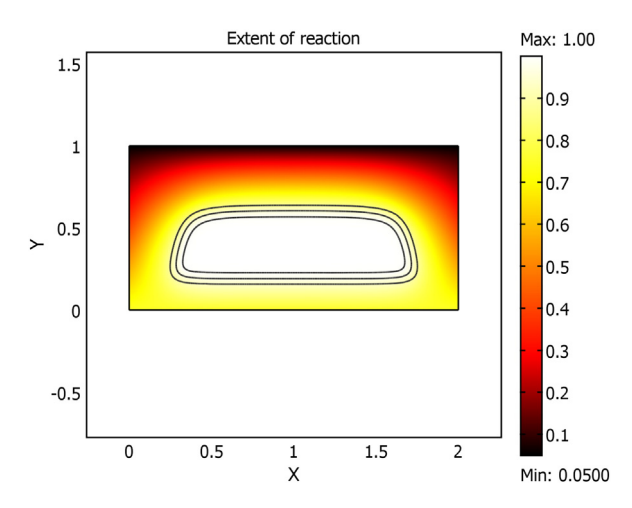


Fig. 7. Model simulation for a weathering block calculated under inhomogeneous boundary conditions: $C^R = 0.05C^e$ at y = 1 and $C^R = 0.75C^e$ at y = 0 ($0 \le x \le 2$); $C^R = (-0.7y + 0.75)C^e$ at x = 0 and x = 2 (see text). Parameters x and y are dimensionless. Dimensionless time equals 0.3. Solute concentration is shown by the color contours. Contour curves (black lines) are shown for the extents of reaction $\eta = 0.9$ (the outer curve), $\eta = 0.5$ (the intermediate curve), $\eta = 0.1$ (the inner curve). This simulation can be considered as a representation of weathering of a corestone or clast embedded in a profile where the solute concentration increases with depth. For such a case, the rock fragment does not weather to a spheroidal corestone; rather, the corestone is trapezoidal as shown. (For interpretation of the references to color in this figure legend, the reader is referred to the web version of this article.)

the block. Given that the chemical affinity of the weathering solution approaches 0 at the bottom, this block weathers slower than an identical block weathering under homogeneous boundary conditions $C^R = 0$ (Fig. 1). In this case, the shape of the weathering front describing the block is not elliptical early in the simulation (for example, at a value of dimensionless time t = 0.3). The clast becomes elliptical only after a longer duration. We infer from this that in general, the rind–core boundaries of naturally weathered clasts often do not have elliptical shapes because they have experienced complex and changing boundary conditions during weathering. These boundaries are expected nonetheless to approach elliptical forms asymptotically with time. The decrease in rind thickness with depth was observed in previous studies of clast weathering (Chinn, 1981; Certini et al., 2003; Hewawasam et al., 2013).

6. Approximation of the model by the Stefan problem and analytical solutions for spherical and cylindrical clasts

As long as we consider weathering in the diffusion-controlled regime (i.e. where $k \to \infty$ and the reaction front is thin), it is possible to consider the front as a surface of discontinuity in the solution of the model described by Eqs. (3)–(4) (Lichtner, 1988; Ortoleva, 1994; Lebedeva et al., 2007). In that case, the problem described in Eqs. (3)–(4) can be approximated as a Stefan problem (Hill, 1987). This approximation presents the reaction front as a moving boundary. With a moving boundary, the model equations considered for j=0, i.e. without reaction, can be solved separately in two domains. One domain includes only the unaltered rock ($\eta=0$) and the outer domain includes only weathered material ($\eta=1$). The mineral alteration reaction only occurs on the surface of discontinuity. Thus, in each domain we need to solve the diffusion equation (we assume that porosity is constant within each domain):

$$\frac{\partial C_i}{\partial t} = D\phi \left(\frac{\partial^2 C_i}{\partial x^2} + \frac{\partial^2 C_i}{\partial y^2} \right), \ i = 1, 2$$
 (20)

where i=1 in the weathered zone and i=2 in the rock. The time evolution of the moving boundary is determined by the jump condition

$$Q^{0} \frac{\partial X}{\partial t} = \left(1 + \left(\frac{\partial X}{\partial y}\right)^{2}\right) \left(D\phi \frac{\partial C_{1}}{\partial x} - D\phi \frac{\partial C_{2}}{\partial x}\right)$$
(21)

$$Q^{0} \frac{\partial Y}{\partial t} = \left(1 + \left(\frac{\partial Y}{\partial x}\right)^{2}\right) \left(D\phi \frac{\partial C_{1}}{\partial y} - D\phi \frac{\partial C_{2}}{\partial y}\right)$$
(22)

where *X* and *Y* are coordinates of the moving boundary f(X, Y, t) = 0 on the plane (x,y).

Eqs. (20)–(22) could be used with an effective diffusion coefficient to treat weathering of low porous material such as obsidian (Anovitz et al., 2004, 2006).

The most important simple analytical estimates of the time evolution of the moving boundary have been previously obtained for the cases of a half-space, a circular cylinder, and a sphere (Hill, 1987):Half-space

$$L = \sqrt{2D\phi\alpha t}. (23)$$

Circular cylinder

$$t = \frac{R_0^2}{4D\phi\alpha} \left(2\left(\frac{R}{R_0}\right)^2 \ln\left(\frac{R}{R_0}\right) + 1 - \left(\frac{R}{R_0}\right)^2 \right). \tag{24}$$

Sphere

$$t = \frac{R_0^2}{6D\phi\alpha} \left(1 - 3\left(\frac{R}{R_0}\right)^2 + 2\left(\frac{R}{R_0}\right)^3 \right). \tag{25}$$

Here, R_0 is the radius of the cylinder or sphere and R(t) and L(t) are the positions of the reaction front at time t. Eqs. (23)–(25) are solutions to the problem under the condition that

$$\alpha = \frac{C^e - C^R}{Q^0} \ll 1 \tag{26}$$

which is typically satisfied for weathering systems. This parameter α is always small because the mass of NaSi $_2$ dissolved in a given mass of pore fluid is always much less than the mass of that component in a unit mass of rock.

Fig. 8 shows the time evolution of the thickness of the weathering rind, $\delta(t) = R_0 - R(t)$ for cylindrical clasts with circular bases of various sizes. The curvature of a circle of radius R is equal to the reciprocal of the radius:

$$|K| = \frac{1}{R}.\tag{27}$$

So it follows from Eq. (24) that the weathering advance rate depends non-linearly on the curvature. Thus, clasts with smaller radii (and greater curvature) weather faster (Fig. 8). Eqs. (24) and (25) allow estimation of the time needed for complete weathering of a cylindrical (t_{cyl}) or spherical (t_{sph}) clast, i.e. the time when R = 0:

$$t_{cyl} = \frac{R_0^2}{4D\phi\alpha} \tag{28}$$

$$t_{sph} = \frac{R_0^2}{6D\phi\alpha}. (29)$$

Formulas (28)–(29) demonstrate that the duration of weathering shows a similar dependence on R_0 , D, ϕ , and α regardless of shape.

These equations are approximate in that they were derived while neglecting the finite reaction rate. Simulations for the model (3)–(8) that do not include the assumption of infinitely fast reaction kinetics show that the duration of complete weathering depends on the rate

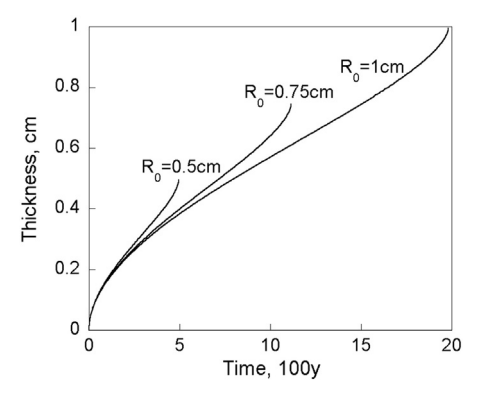


Fig. 8. Calculated time evolution plots for weathering rinds of circular cylinders of various radii, R_0 . The parameters are as follows (Eqs. (24) and (26)): $D=0.8\cdot 10^{-9}$ m²/s, $\phi=0.1$, $\alpha=5\cdot 10^{-7}$. The curves terminate at the point where the clast (represented as a cylinder) has completely weathered. The figure documents that over some interval during weathering of each clast, thickness increases approximately as a linear function of time, as has been observed for some natural systems (Sak et al., 2004). In addition, the rate of thickneing (derivative of the thickness with respect to time) is faster for smaller clasts than larger clasts. In effect, smaller clasts weather away faster for both because they are smaller and because of the curvature effect. Finally, the effect of curvature and clast size is negligible during initial weathering but becomes more important with increasing weathering duration.

constant, i.e., the duration is less for a faster weathering reaction, as expected. Therefore, estimates (28)–(29) for the transport-limited case yield only the minimal weathering time.

Another important question we can address is the error that is incurred when a clast of any arbitrary shape is approximated as a cylindrical or spherical clast. For example, an attempt to use a modified form of Hill's Eq. (25) for a spherical clast was undertaken in a recent paper (Reeves and Rothman, 2014). The authors argued that this approximation is applicable to any irregular clast. However, calculations presented in the appendix document that depending on the shape of the clast, the approximation leads to deviations from the actual duration of weathering that can be as large as 30%. For complicated geometries, solutions must be found numerically. For solidification of material approximated as rectangles or rectangular parallelepipeds, asymptotic solutions have been previously described (McCue et al., 2003, 2005). We modified this approach and applied it to weathering problems (see Appendix C). These approximations (Eq. (C.1)) lead to more satisfactory estimates than Eqs. (28)–(29).

7. Discussion and results

The model can also be used to explore the effect of porosity on clast weathering. The porosity calculated across the core–rind boundary for the Guadeloupe clast (Sak et al., 2010) is presented in Fig. 9a. Porosity of the rind is much greater than porosity of the core. On a transect across the rind–core interface, the porosity first slightly decreases, then

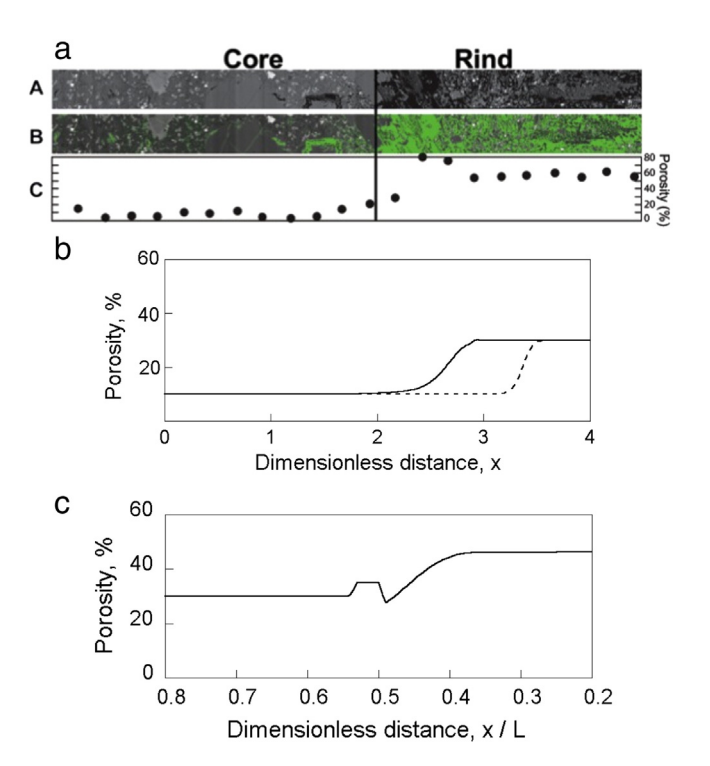


Fig. 9. a. Porosity map (labeled C) across the core-rind boundary for the Guadeloupe clast (Sak et al., 2010). Images of the thin section are shown in A under back-scattered electron microscopy (brighter grains are denser). Pore space is shown in green in B as measured under secondary electron microscopy using an FEI Quanta 400 environmental SEM. b. Porosity calculated along the vertical axis (denoted x here) of the elliptical clast shown in Fig. 3 (solid curve) and along the x-axis of the 1-D slab (dashed curve) for a model with diffusion only. Note that the reaction front is thicker for the curved front as compared to the planar front. Similarly, as discussed in the text, reaction fronts are thicker for diffusion + advection models than for diffusion-only models for similar model conditions (Lebedeva et al., 2010). c. Porosity calculated for a 4-mineral model (Brantley et al., 2014) showing that the inclusion of multiple minerals reacting can produce "bumps" in porosity versus position curves. The model for the simulation shown here included non-reacting quartz, albite reacting to kaolinite and FeO reacting to goethite. Loss of porosity along the transect is attributed to goethite precipitation. (For interpretation of the references to color in this figure legend, the reader is referred to the web version of this article.)

increases at the mineral alteration front and diminishes within the intact core. The simulations of porosity (Fig. 9b) for the elliptical clast presented in Fig. 3 (solid curve) and for the 1-D slab (dashed curve) look similar to the natural curve although the functions change monotonically without the "bump" in porosity documented in the clast itself (Fig. 9a). Although calculated porosities for the elliptical clast and for the slab both change monotonically, the dependence of the front velocities on time differs: the front velocity for the elliptical clast is almost constant in some time interval in Fig. 4(a) (even though the simulation does not include advection) while the front velocity for the slab diminishes with time as $t^{-0.5}$ (not shown) according to Eq. (13). Therefore, it is not necessary to invoke changes in porosity to account for deviations from the parabolic law, as was previously argued (Navarre-Sitchler et al., 2011). According to our treatment, a change in porosity affects the effective diffusion coefficient, $D_{eff} = Df(\phi)$ ($D_{eff} = D\phi$ in Eq. (13)) but does not explain why the non-linear time dependency, i.e., L =

 $2c\sqrt{t}$, $\omega = c/\sqrt{t}$ (where $c = \sqrt{0.5D_{eff}(C^e - C^R)/Q^0}$), becomes linear, i.e. $L = \omega t$, $\omega = const$. In fact, the threshold model (Navarre-Sitchler et al., 2011) only changes the coefficient c.

The simple, monotonic variation in modeled porosity as a function of distance across the reaction front in both the elliptical clast and the slab is likely related to the model being limited to alteration of only one mineral. Even a slightly more complex model that simulated 4 minerals (Brantley et al., 2014) produced a more complex distribution of porosity within the weathering system, including zones where porosity "bumps" are observed (Fig. 9c). Regardless, however, the two planar fronts simulated by Brantley et al. (2014) both move with a parabolic dependence on time following Eq. (13). Thus, curvature exerts a first order control in the advance of weathering fronts for clasts with low initial porosity.

We have presented the first numerical and analytical investigation of curvilinear weathering fronts using a simple 2-D approximation of a multi-mineral multicomponent reaction-diffusion model for weathering clasts. The model describes the following observations about rind formation: i) the core-rind boundary rounds with time; ii) the transition from unweathered core to weathered rind occurs over a narrow zone (which we call a weathering reaction front); iii) the front is characterized by an increase in porosity; and iv) the rate of weathering advance (distance/time) is faster where the curvature is higher. Our results are in agreement with measurements (Sak et al., 2010; Ma et al., 2012). In particular, it has been observed in those papers that the rind and front thicknesses vary with the absolute value of curvature of the weathering fronts. Our approach shows that the weathering rind and front thicknesses that develop on a weathering clast are directly proportional to the absolute value of the curvature of the weathering front.

Similar mathematical problems arise for other natural phenomena. Although their physical origins are diverse, the mathematical similarity allows analysis based on methods in the literature. Here we have applied them to weathering. Applying the previous analysis presented in the literature (Entov and Etingof, 1991; McCue et al., 2003) to weathering of clasts of any shape, we conclude that the core–rind boundary of the clast will ultimately approach an ellipse just before complete weathering. Our numerical simulations document this result. This result has an important implication allowing a quick estimation of weathering duration. The non-elliptical shape corresponds with the beginning stage of weathering while the form close to the ellipse means that weathering is close to completion. In this case, the weathering duration could be estimated using the approximate Eqs. (28), (29), and (C.1).

The model presented here is a mesoscale model that implicitly averages over microscale features such as grain size or porosity. Examples of investigations of pore-scale reaction rates, i.e. mineral alteration fronts on micro-scales, have been presented previously (Putnis, 2009; Levenson and Emmanuel, 2013). For example, the micro-images obtained previously (Putnis, 2009) document curvilinear fronts of mineral

replacement on single crystals. Other researchers have suggested that differences in reaction rates that have been observed could be due to the effect of curvature at the micro-scale where the rate of dissolution could increase or decrease depending on the geometry of the surface (Levenson and Emmanuel, 2013), i.e., similar to our simulations in Fig. 5.

Variations in grain size and porosity can also contribute to weathering advance and may explain some differences in weathering advance rates in materials that differ significantly in grain size and porosity such as obsidian (Anovitz et al., 2004), sandstone (Chinn, 1981; Certini et al., 2003), and basaltic substrates (Sak et al. (2010), Ma et al. (2012)). We can make some inferences from our model about weathering of other rock types if we assume that albite in the model represents any abundant mineral that is weathering and that quartz represents the non-reactive part of the rock. For example, weathering of very pure sandstone (very quartz-rich and lithic fragment-poor) is mostly due to dissolution of cement. To apply our model to such a sandstone, the cement in the rock could be considered equivalent to the model feldspar. The major difference would be the mol % of cement (i.e. feldspar) would be very low in the clast starting material. This would enhance the effect of curvature according to Eq. (15). For example, if only 2% of feldspar is present, then the effect of curvature increases 2.5 times in comparison to the example in Fig. 3 where 5% of albite is initially present. Local rind thickening at the sharp corners of angular clasts of sandstones has been observed (Chinn, 1981) in accordance with Fig. 2.

Although grain size is not included explicitly in our model, smaller grain size results in higher specific surface area and effective rate constant (Eq. (A.9)). Clasts with smaller grain size are thus expected to weather faster. For example, clasts formed from intrusive igneous rocks of a given composition should demonstrate lower rates of rind formation than equivalent extrusive rocks weathering under similar environmental conditions. Furthermore, clasts with variations in grain size could show variations in rind and front thickness related to grain size in addition to the effects of curvature. Specifically, the grain size can affect porosity and transport conditions. For example, if grain size enhances the effective diffusivity, then rind growth may be affected (Chinn, 1981).

We modeled clasts with homogeneous weathering rinds. Nonetheless in the natural systems there are observed more complex weathering patterns. For example, alteration on a basalt boulder has been described that has different colored concentric diffusion rings following the shape of the boulder (Singer and Navrot, 1970). For future work, such a system might be modeled using two separate reactions (A.13)–(A.14) and by applying the conditions for ring formation obtained previously (Lebedeva et al., 2004).

8. Conclusions and implications

From the model equations, a linear relationship between the normal velocity of the curvilinear weathering front, ω_n , and the curvature of the weathering front, K, was derived:

$$\omega_n = \omega_0 - \beta K. \tag{30}$$

Here ω_0 is the velocity of a planar reaction front (i.e., K=0) and β is a parameter characterizing chemical, physical, and transport parameters for the modeled system: $\beta = (D\phi(C^e - C^R)/Q^0)$. Thus, the velocity of weathering front (weathering advance rate measured in distance/time) is determined not only by mineralogical content (Q^0), solute concentration ($C^e - C^R$), solute transport characteristics (D, v), and porosity (ϕ), but also by the curvature of the weathering front K.

The weathering front velocity depends on the sign of curvature and can therefore be greater or lower than the velocity of a front that is planar. Particularly, for diffusion-only transport the velocity of weathering front depends on time as $t^{-0.5}$ (Eq. (13)). We obtained that the velocity of the curvilinear front is almost constant in time. For the 1-D planar

front the velocity is constant when the reactive transport occurs by both diffusion and advection (Eq. (12)). Therefore, in diffusion-reactive processes, the effect of curvature results in a mathematical description that is similar to that derived based on the assumption that the dominant solute transport mechanism is advection. In other words, the curvilinear core–rind boundary advances at a rate that is independent of time rather than parabolic. This could be the explanation for the complex time dependence of rind thickness for clasts that has been previously discussed (Sak et al., 2004; Ma et al., 2012). Importantly, this improved reconstruction of the time dependencies of rind thicknesses allows better estimations of the time durations of exposure to weathering.

The boundary conditions at the surface of the clast (solute concentration, fluxes of components in the pore fluid) affect the curvature and velocity of advance of the weathering front. Therefore, if solute concentrations and fluxes vary with depth, it could be important to take into account the locations of weathering clasts within regolith profiles when analyzing field observations. We show in Section 4 how the difference in curvature in different locations of the core—rind boundary can be used to estimate duration of clast weathering.

Our simulations document that using cylindrical and spherical approximations of an arbitrary clast could lead to errors as large as 30% even if the parameters of the kinetic function are known. Simple local-equilibrium approximations for the time evolution of the corerind boundary — i.e., solutions of the Stefan problem for slabs, circular cylinders, and spheres — could also be inaccurate. In these cases the model must be solved numerically. But for rectangular corestones or clasts, we present modified versions of the more complex analytical expressions that have previously been obtained for a different physical phenomenon (McCue et al., 2003, 2005). These modified expressions could be applied to weathering problems to reduce the inaccuracies of the cylindrical and spherical approximations.

Given that weathering generally causes rocks to break up into smaller objects — blocks, corestones, clasts, grains — a complete understanding of the time dependence of weathering will only be possible if the effects of curvature are explored and incorporated in future model treatments. We define weathering as transformation of a rock to soil. To our knowledge, there are no geochemical models that incorporate the consideration that during weathering, the rock typically decreases in grain size (or equivalently, increases in specific surface area). Our model is a step toward understanding how to quantitatively deal with changes in texture during weathering. One of the remaining first-order puzzles in geology is the question "How thick is soil in any location and what controls this thickness?" Our modeling efforts reported here can be considered as one way to explore this question, i.e. by simplifying the modeled soil system to that of a weathering rind on a clast. We study clasts in this paper as a first-step toward understanding what controls the thickness of soil. Soil formation is classically thought to rely on factors including climate, parent material, biota, relief, and time. We argue that front curvature should be considered as an aspect that contributes to controlling rates of formation.

Acknowledgments

This work was funded by the U.S. Department of Energy Office of Basic Sciences grant DE-FG02-OSER15675 to SLB. LM and PBS acknowledge partial funding from the National Science Foundation grants EAR-1251952 and EAR-1251969.

Appendix A. Origin of the approximate model

The model of weathering granite bedrock is described through the reactions:

$$NaAlSi_3O_{8(ab,s)} + H^+_{(aq)} + H_2O \rightleftharpoons Na^+_{(aq)} + Al(OH)_{3(aq)} + 3SiO_{2(aq)}$$
 (A.1)

$$\text{FeO}_{(s)} + 2\text{H}_{(aq)}^+ \rightleftharpoons \text{Fe}_{(aq)}^{2+} + \text{H}_2\text{O}$$
 (A.2)

$$Al_{2}Si_{2}O_{5}(OH)_{4(kao.s)} + H_{2}O \rightleftharpoons 2Al(OH)_{3(aq)} + 2SiO_{2(aq)} \tag{A.3} \label{eq:A.3}$$

$$FeO(OH)_{(gth,s)} + 2H_{(aq)}^{+} \rightleftharpoons \frac{1}{4}O_{2(aq)} + Fe_{(aq)}^{2+} + \frac{3}{2}H_{2}O.$$
 (A.4)

We assume that precipitation of goethite (gth), FeO(OH) and kaolinite (kao), $Al_2Si_2O_5(OH)_4$, after dissolution of albite (ab), forms the weathering rind. Additionally, we consider the following homogeneous reactions for aqueous species:

$$H_{(aq)}^{+} + OH_{(aq)}^{-} \rightleftharpoons H_{2}O \tag{A.5}$$

$$Fe_{(aq)}^{3+} + \frac{1}{2}H_2O \rightleftharpoons H_{(aq)}^+ + \frac{1}{4}O_{2(aq)} + Fe_{(aq)}^{2+}. \tag{A.6}$$

The reaction rate, j_j , is described by a generalized kinetic equation for mineral dissolution or precipitation and is expressed as the product of three functions:

$$j_{j} = f_{j}(s_{j})k_{j}(a_{aq}; \overline{E}_{Aj})\Psi_{j}(\overline{A}_{j})$$
(A.7)

where j_i is positive for mineral dissolution.

The function $f_j(s_j)$ determines the reaction rate dependence on the specific surface area s_j of given mineral j. For Eqs. (A.1) through (A.4), j = ab, FeO, kao, and gth. We assume that $f_j(s_j) = s_j$. The value of s_i (m⁻¹) is calculated as the geometric surface area:

$$s_i = 6n_i^{1/3}\phi_i^{2/3} \tag{A.8}$$

where n_j (m⁻³) is the number of mineral grains per unit volume of a porous medium. We define this as

$$n_j = \frac{\phi_j^*}{\left(d_{gj}^*\right)^3}.\tag{A.9}$$

Here, d_{gj}^* (m) is the average size of mineral grains at a characteristic volume fraction, ϕ_j^* . Based upon observations and models for weathering of a Puerto Rico quartz diorite (Buss, 2006), we set d_{gj}^* to a nominal value of 10^{-4} m at $\phi_j^* = 0.2$ for albite, kaolinite, and FeO while $d_{gj}^* = 5 \cdot 10^{-6}$ m at $\phi_j^* = 0.1$ for goethite.

A transfer of components between solid and fluid phases is described by the kinetic function $k_j(a_{aq}; \bar{E}_{Aj})$ where a_{aq} is the activity vector of aqueous species and $\bar{E}_{Aj} = E_{Aj}/RT$, where E_{Aj} is the activation energy, R is the universal gas constant, and T is absolute temperature. According to the work of many researchers to describe silicate dissolution (Brantley, 2004), the kinetic function k_j is expressed as follows:

$$k_{j}\left(a_{aq};\overline{E}_{Aj}\right) = k_{j}^{0} \exp\left(-\overline{E}_{Aj}\right) \left(a_{H^{+}}^{h_{1j}} + \kappa_{j} a_{OH^{-}}^{h_{2j}} + h_{3j}\right) \tag{A.10}$$

where k_j^0 , $k_j^0 \kappa_j$ and $k_j^0 h_{3j}$ are the rate constants for proton-promoted, hydroxyl-promoted, and H₂O-promoted dissolution respectively, measured at pH 0 and 298 K for the reaction of interest. The parameters h_{1j} and h_{2j} are constants that represent the partial reaction order with respect to H⁺ and OH⁻ respectively.

To describe reaction rate as a function of chemical affinity \bar{A}_j we use the standard function Ψ_j :

$$\Psi_{j}(\overline{A}_{j}) = 1 - \exp(-\overline{A}_{j}) \tag{A.11}$$

where

$$\overline{A}_j = A_j/RT, \ \overline{A}_j = \ln(\prod_i a_i^{\nu_{ji}}/K_j),$$
 (A.12)

 $\nu_{ji} = \nu_{ji}^+ - \nu_{ji}^-$, ν_{ji}^- and ν_{ji}^+ are the stoichiometric coefficients for the leftand right-hand side of the chemical reaction respectively, and K_j are the equilibrium constants of the reactions.

Analysis of the numerical solutions of the model (A.1)–(A.6) (Lebedeva et al., 2007) shows that instead of the reaction system (A.1)–(A.6) we can write two main reaction equations:

$$\text{FeO}_{(s)} + \frac{1}{4}O_{2(aq)} \xrightarrow{\frac{1}{2}H_2O} \text{gth}$$
 (A.13)

$$2ab \xrightarrow{3H_2O} kao + 2(Na^+_{(aq)} + OH^-_{(aq)} + 2SiO_{2(aq)}).$$
 (A.14)

In other words, the more complex multi-component scheme (A.1)–(A.4) can be split into the two independent one-component reactions (A.13) and (A.14). Comparison of the numerical solutions (Lebedeva et al., 2007) of the full and approximate models allows derivation of the approximate kinetic function and calculation of the effective kinetic constant.

In a previous publication (Lebedeva et al., 2007), the 1-D model for reaction (A.13) only was analyzed. The 1-D model for reaction (A.14) was also considered previously (Lebedeva et al., 2010). Here we also focus on reaction (A.14).

Appendix B. Analysis of the curvilinear reaction front

We can show the effect of curvature mathematically using model Eqs. (3)–(4) and a technique described in the literature (Zykov, 1980; Keener, 1986; Grindrod, 1991). We introduce local orthogonal curvilinear coordinates (ξ, λ) that allow us to reduce the problem from 2-D to 1-D: λ describes contour lines for the variables (C, η) , i.e. a moving interface for mineral alteration. (A contour curve is the curve where the extent of reaction is constant.) The ξ coordinate is the characteristic line describing weathering advance (Aris and Knapp, 1972) (Fig. B.1). In this coordinate system, we can replace the 2-D Eqs. (3)–(4) by the 1-D equations (see Zykov, 1980; Keener, 1986; Grindrod, 1991 for details):

$$\frac{\partial (\phi C)}{\partial t} = \frac{\partial}{\partial \varepsilon} \left(D\phi \frac{\partial C}{\partial \varepsilon} \right) + KD\phi \frac{\partial C}{\partial \varepsilon} + j(C, \eta) \tag{B.1}$$

$$\frac{\partial \eta}{\partial t} = \frac{j(C, \eta)}{Q^0}.$$
 (B.2)

Here K is curvature of the contour curve defining the weathering front (for example, the contour curve at $\eta = 0.5$). By comparing Eq. (B.1) to Eq. (10), we see that the term including curvature K is

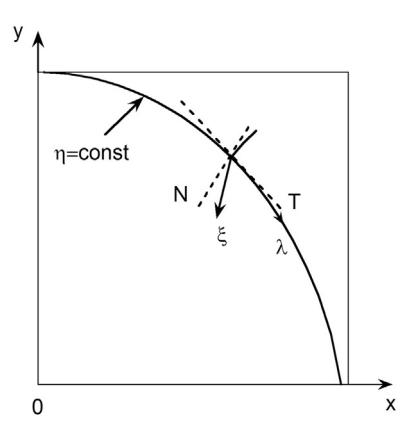


Fig. B.1. The local curvilinear system of coordinates (ξ, λ) . The curve $\eta = const$ is the contour curve. T is the tangent line and N is the normal line to the curve at a given point. Curvature of the contour curve as shown is negative. Here, the rock clast is on the left and the environment is on the right.

similar to the term in the earlier equation for advection. So for a curvilinear weathering front with constant curvature K < 0, the normal component of the weathering advance rate is calculated by Eq. (12) with $v = D\phi |K|$.

Appendix C. Geometrical approximation and approximation of the model by the Stefan problem

Here, we use numerical simulations to estimate the error that is incurred when a clast of an arbitrary shape is approximated as a cylindrical or spherical clast. To assess this, we considered two examples: weathering blocks with either rectangular or square bases which have identical heights equal to unity. Each clast was approximated as a circular cylinder of the same volume as the corresponding block. First we estimate the error in the case when the kinetic function is known and it is possible to calculate the exact complete weathering time for each clast. We solve the original reaction-diffusion problem (3)–(4) and calculate the time of complete weathering. We use identical reaction kinetics (Eqs. (7)–(8)). For this case, we obtained T_{block} = $0.74T_{cyl}$ and $T_{block} = 0.96T_{cyl}$ for the rectangular and square block, respectively. T_{block} and T_{cyl} are the dimensional weathering times for the block and cylinder, respectively. Thus, depending on the shape of the clast, the approximation leads to different results such that the deviation from the actual duration of weathering ($|T_{block} - T_{cyl}|/T_{block}$) could be as large as 30%. So for numerical modeling and accuracy better than tens of percent, it is important to consider geometry of weathering clasts as close to real as possible.

Next we compare the results of a numerical solution and the approximation by the Stefan problem for a rectangular block of size $0 \le x \le a$, $0 \le y \le b$ (base). Simulation (i.e., solution of Eqs. (3)–(8)) for $kb^2/D=400$ yields $t_e^{calc}=3.4\cdot 10^5y$. In comparison, from Eq. (28) we obtain $t_e^{cyl}=4.2\cdot 10^5y$ for a cylinder with radius $R_0=\sqrt{ab/\pi}$.

The estimation can be improved using approximate analytical solutions for rectangles and rectangular parallelepipeds. These solutions have been previously described (McCue et al., 2003, 2005) for a solidification problem.

Following their method we estimate the complete weathering time for a rectangular block of size $0 \le x \le a$, $0 \le y \le b$ as

$$\begin{split} &t_{e} \! \approx \! \frac{b^{2}Q^{0}}{4D\phi(C^{e}\!-\!C^{R})} \left(\! \frac{1}{2} \! - \! \sum_{m=0}^{\infty} \! \frac{16(-1)^{m}}{\pi^{3}(2m+1)^{3} \cosh(0.5(2m+1)\pi a/b)} \! \right) \\ &\approx \! \frac{b^{2}Q^{0}}{4D\phi(C^{e}\!-\!C^{R})} \left(\! \frac{1}{2} \! - \! \frac{16}{\pi^{3} \cosh(0.5\pi a/b)} \! \right) \! . \end{split} \tag{C.1}$$

Applying this equation to the weathering block in Fig. 1 we obtain $t_e=3\cdot 10^5 y$ (for $a=2\,$ m, $b=1\,$ m, $D=0.8\cdot 10^{-9}\,$ m $^2/s$, $\phi=0.3$, $Q^0=4\cdot 10^3\,$ mol/m 3 , $C^e=0.2\,$ mol/m 3 , $C^R=0$).

Thus Eq. (C.1) presents a satisfactory estimate. This estimate could be improved by including more terms in Eq. (C.1) and using additional terms obtained by (McCue et al., 2003).

References

- Anderson, S.P., Dietrich, W.E., Brimhall, G.H.J., 2002. Weathering profiles, mass-balance analysis, and rates of solute loss: linkages between weathering and erosion in a small, steep catchment. GSA Bull. 114 (9), 1143–1158.
- Anovitz, L.M., Elam, J.M., Riciputi, L.R., Cole, D.R., 2004. Isothermal time-series determination of the rate of diffusion of water in Pachuca obsidian. Archaeometry 46 (2), 301–326.
- Anovitz, L.M., Riciputi, L.R., Cole, D.R., Fayek, M., Elam, J.M., 2006. Obsidian hydration: a new paleothermometer. Geology 34 (7), 517–520.
- Aris, R., Knapp, R.H., 1972. On the equations for the movement and deformation of a reaction front. Arch. Ration. Mech. Anal. 44 (3), 165–177.
- Brantley, S.L., 2004. Reactions kinetics of primary rock-forming minerals under ambient conditions. In: Drever, J.I. (Ed.), Surface and Ground Water, Weathering, and Soils. 5. Elsevier Pergamon, Oxford, pp. 73–117.
- Brantley, S.L., White, A.F., 2009. Approaches to Modeling Weathered Regolith. Thermodynamics and Kinetics of Water–Rock Interaction. In: Oelkers, E.H., Schott, J. (Eds.), Mineral. Soc. Am. 70, pp. 435–484

- Brantley, S.L., Lebedeva, M.I., Bazilevskaya, E.A., 2014. Relating Weathering Fronts for Acid Neutralization and Oxidation to pCO₂ and pO₂. In: Farquhar, J., Kasting, J., Canfield, D. (Eds.), Treatise Geochem. 6. Elsevier, Amsterdam, The Netherlands, pp. 327–352
- Brazhnik, P.K., Tyson, J.J., 1999. Velocity-curvature dependence for chemical waves in the Belousov–Zhabotinsky reaction: theoretical explanation of experimental observations, Phys. Rev. E 59 (4), 3920–3925.
- Brimhall, G.H., Dietrich, W.E., 1987. Constitutive mass balance relations between chemical composition, volume, density, porosity, and strain in metasomatic hydrochemical systems: results on weathering and pedogenesis. Geochim. Cosmochim. Acta 51, 567–587.
- Buss, H.L., 2006. Biogeochemical Weathering of Iron-Silicate Minerals. Ph.D. Thesis, University Park, The Pennsylvania State University (Ph.D.: 203).
- Cernohouz, J., Solc, I., 1966. Use of sandstone wanes and weathered basaltic crust in absolute chronology. Nature 212, 806–807.
- Certini, G., Hillier, S., McMurray, E., Edwards, A.C., 2003. Weathering of sandstone clasts in a forest soil in Tuscany (Italy). Geoderma 116, 357–372.
- Chinn, T.J.H., 1981. Use of rock weathering-rind thickness for Holocene absolute agedating in New Zealand. Arct. Alp. Res. 13 (1), 33–45.
- Chou, L., Wollast, R., 1985. Steady-state kinetics and dissolution mechanism of albite. Am. I. Sci. 285, 963–993.
- Colman, S.M., 1982. Clay mineralogy of weathering rinds and possible implications concerning the sources of clay minerals in soil. Geology 10, 370–375.
- Colman, S.M., Pierce, K.L., 1981. Weathering rinds on andesitic and basaltic stones as a Quaternary age indicator, Western United States. U.S. Geological Survey 1210. COMSOL, 2008. Multiphysics User's Guide.
- Entchev, P.B., Lagoudas, D.C., Slattery, J.C., 2001. Effect of non-planar geometries and volumetric expansion in the modeling of oxidation in titanium. Int. J. Eng. Sci. 39, 695–714
- Entov, V.M., Etingof, P.I., 1991. Bubble contraction in Hele–Shaw cells. Q. J. Mech. Appl. Math. 44. 509–535.
- Fletcher, R.C., Brantley, S.L., 2010. Reduction of bedrock blocks as corestones in the weathering profile: observations and model. Am. J. Sci. 310, 131–164.
- Foester, P., Muller, S.C., Hess, B., 1988. Curvature and propagation velocity of chemical waves. Sci. New Ser. 241 (4866), 685–687.
- Grindrod, P., 1991. Patterns and Waves: The Theory and Applications of Reactiondiffusion Equations. Clarendon Press, New York.
- Hellman, R., 1994. The albite-water system: Part 1. The kinetics of dissolution as a function of pH at 100, 200, and 300 °C. Geochim. Cosmochim. Acta 58 (2), 595–611.
- Hewawasam, T., von Blanckenburg, F., Bouchez, J., Dixon, J.L., Schuessler, J.A., Maekeler, R., 2013. Slow advance of the weathering front during deep, supply-limited saprolite formation in the tropical highlands of Sri Lanka. Geochim. Cosmochim. Acta 118, 202–230.
- Hill, J.M., 1987. One-dimensional Stefan Problem: An Introduction. Wiley & Sons, New York.
- Keener, J.P., 1986. A geometrical theory for spiral waves in excitable media. SIAM J. Appl. Math. 46 (6), 1039–1056.
- Kirkbride, M.P., 2005. Boulder edge-roundness as an indicator of relative age: a Lochnagar case study. Scott. Geogr. J. 121 (2), 219–236.
- Kirkbride, M.P., Bell, S.M., 2010. Edge-roundness of boulders of Torridonian Sandstone (northwest Scotland): applications for relative dating and implications for warm and cold climate weathering rates. Boreas 39, 187–198.
- Knapp, R.H., Aris, A., 1972. On the equations for movement and deformation of a reaction front. Arch. Ration. Mech. Anal. 44, 165–177.
- Lebedeva, M.I., Brantley, S.L., 2013. Exploring geochemical control on weathering and erosion of convex hillslopes: beyond the empirical regolith production function. Earth Surf. Process. Landf. http://dx.doi.org/10.1002/esp.3424.
- Lebedeva, M.I., Vlachos, D.G., Tsapatsis, M., 2004. Pattern formation in porous media via the Liesegang Ring Mechanism. Ind. Eng. Chem. Res. 43, 3073–3084.
- Lebedeva, M.I., Fletcher, R.C., Balashov, V.N., Brantley, S.L., 2007. A reactive-diffusion model describing transformation of bedrock to saprolite. Chem. Geol. 244, 624–645.
- Lebedeva, M.I., Fletcher, R.C., Brantley, S.L., 2010. A mathematical model of steady-state regolith production at constant erosion rate. Earth Surf. Process. Landf. 35, 508–524.
- Levenson, Y., Emmanuel, S., 2013. Pore-scale heterogeneous reaction rates on a dissolving limestone surface. Geochim. Cosmochim. Acta 119, 188–197.
- Lichtner, P.C., 1988. The quasi-stationary state approximation to coupled mass transport and fluid-rock interaction in a porous medium. Geochim. Cosmochim. Acta 52, 143–165.
- Ma, L., Chabaux, F., Pelt, E., Granet, M., Sak, P.B., Gaillardet, J., Lebedeva, M.I., Brantley, S., 2012. The effect of curvature on weathering rind formation: evidence from uranium-series isotopes in basaltic andesite weathering clasts in Guadeloupe. Geochim. Cosmochim. Acta 80, 92–107.
- Markstein, G.H., 1951. Experimental and theoretical studies of flame front stability. J. Aerosol Sci. 18, 199–209.
- McCue, S.W., King, J.R., Riley, D.S., 2003. Extinction behaviour for two-dimensional inward-solidification problems. Proc. R. Soc. Lond. A 459, 977–999.
- McCue, S.W., King, J.R., Riley, D.S., 2005. The extinction problem for three-dimensional inward solidification. J. Eng. Math. 52, 389–409.
- Navarre-Sitchler, A., Steefel, C.I., Sak, P.B., Brantley, S.L., 2011. A reaction-transport model for weathering rind formation on basalt. Geochim. Cosmochim. Acta 75, 7644–7667.
- Neretnieks, I., 1980. Diffusion in the rock matrix: an important factor in radionuclide retardation? J. Geophys. Res. 85 (B8), 4379–4397.
- Oguchi, C.T., 2004. A porosity-related diffusion model of weathering-rind development. Catena 58, 65–75.
- Ortoleva, P.J., 1994. Geochemical Self-organization. Clarendon Press, Oxford.
- Ortoleva, P.J., Chadam, J., Merino, E., Sen, A., 1987. Geochemical self-organization II: the reactive-infiltration instability. Am. J. Sci. 287, 1008–1040.

- Putnis, A., 2009. Mineral replacement reactions. In: Oelkers, E.H., Schott, J. (Eds.), Rev. Mineral. Geochem. 70, pp. 87–124
- Reeves, D., Rothman, D.H., 2014. Diffusion and kinetic control of weathering layer development. Geofluid 14, 128–142.
- Ruxton, B.P., Berry, L., 1957. Weathering of granite and associated erosional features in Hong Kong. GSA Bull. 68, 1263–1292.
- Sak, P.B., Fisher, D.M., Gardner, T.W., Murphy, K., Brantley, S.L., 2004. Rates of weathering rind formation on Costa Rican basalt. Geochim. Cosmochim. Acta 68, 1453–1472.
- Sak, P.B., Navarre-Sitchler, A., Miller, C.E., Daniel, C.C., Gaillardet, J., Buss, H.L., Lebedeva, M.I., Brantley, S.L., 2010. Controls on rind thickness on basaltic andesite clasts weathering in Guadeloupe. Chem. Geol. 276, 129–143.
- Sidborn, M., Neretnieks, I., 2007. Long term redox evolution in granitic rocks: modelling the redox front propagation in the rock matrix. Appl. Geochem. 22, 2381–2396.
- Singer, A., Navrot, J., 1970. Diffusion rings in altered basalt. Chem. Geol. 6, 31–41.
- Soler, J.M., Lasaga, A.C., 1998. An advection-diffusion-reaction model of bauxite formation. J. Hydrol. 209, 311–330.

- Steefel, C.I., Lichtner, P.C., 1994. Diffusion and reaction in rock matrix bordering a hyperalkaline fluid-filled fracture. Geochim. Cosmochim. Acta 58 (17), 3595–3612.
- Wang, Y., Wang, Y., Merino, E., 1995. Dynamic weathering model: constraints required by coupled dissolution and pseudomorphic replacement. Geochim. Cosmochim. Acta 59 (8), 1559–1570.
- White, A.F., 2002. Determining mineral weathering rates based on solid and solute weathering gradients and velocities: application to biotite weathering in saprolites. Chem. Geol. 190, 69–89.
- Zaraisky, G.P., Balashov, V.N., Lebedeva, M.I., Soboleva, Y.B., 2002. Experimental Metasomatic Column as a Tool for Securing of Kinetic Constants of Metasomatic Reactions. 1. Herald of the Earth Sciences Department RAS.
- Zeldovich, Y.B., 1981. Structure and stability of steady laminar flame at moderately large Reynolds numbers. Combust. Flame 40, 225–234.
- Zykov, V.S., 1980. Analytical evaluation of the dependence of the speed of excitation wave in a two-dimensional excitable medium on the curvature of its front. Biophysics 25, 906–911.